Chemistry and Materials Research
ISSN 2224- 3224 (Print) ISSN 2225- 0956 (Online)
Vol.7 No.12, 2015

The effect of temperature on preparation of nano material via dopping ZP in mesoporous activated carbon

*N.El-said M.M.S.Ali and A.T.Kassem
Atomic Energy Authority, Hot Labs. Center, P.Code 13759, Cairo, Egypt

ABSTRACT

A nano material was obtained by dopping ZP in mesoporous nanocarbon which prepared by physical activation carbon via thermal effect .A series of ZP materials dopped in activated carbon obtained from DP by physical activation. The dopped ZP-C materials were heat-treated at various temperatures, 100–800 ^{0}C. TGA & DTG thermal analysis showed that incorporation of the doping agent within the carbon DP layered materials which enhanced the heat-resistivity of the nanohybrid materials in the thermal decomposition pathway. Porous carbon materials can be obtained from the heat-treatment of the nanohybrids at 700 and 900 ^{0}C. Calcination of the dopped material was achieved at 900^{0}C under nitrogen atmosphere which produces mesoporous and high pore volume carbon materials. According to the kinetics of Freeman–Carroll and Coats–Redfern the calculated order of reaction of ZP in DP is 2. The calculated activation energy of both matrices are 402 and 350 kJ mol^{-1}.

Key Words: Activated carbon; solid waste DP; physical activation; ZP; and nanotechnology

1. INTRODUCTION

The key to dynamic analysis of thermal decomposition is to determine mechanism of solid reactions and to obtain kinetic parameters. Theoretical analysis methods include differential method, integral method and the integration of the both methods. Experimental techniques include isothermal methods and the non-isothermal methods which are more popular than the former [Flynn. J.H.(1996).]. It should be noted that the dynamic parameters derived from varying method are sometimes quite different [Hornyak. G.L et al (1999)]. The Ozawa method is well documented to be the most useful one to obtain decomposition activation energy [Ozawa .T.(1965)& Flynn. J.H.(1996).]. Using this method, there is no Carbon fiber-reinforced composites (ceramic, glass**,** glass–ceramic and polymers, abbreviated as CFRCs) have received much attention in recent years. Their good mechanical, thermal and chemical properties, especially from the point of view of property/weight and property/cost ratios, make these materials widely applicable in many fields. Recently, attention has been focused on three-dimensional (3-D) braided carbon fiber-reinforced composites in order to meet mechanical and thermal properties requirements along the thickness of the composites [Xu.Y, Lin. Z, Huang .X, et al.(2013). 5], although it has many advantages, such as low specific weight, and excellent mechanical strength at elevated temperatures. Consequently, the applications of CFRCs as high-temperature material have been mostly limited to inert atmosphere in order to prevent the oxidation degradation of carbon fiber [Yin. Y, Binner.et al. (1994)& Zhao. L.R,et al.(1997)]. Once the interfacial bond between fiber and matrix has been deboned by oxidation, a significant reduction in mechanical properties of the composite is unavoidable [Bullions.T.A,et al.(2003)& Labruquére.S,et al.(2002)].There have been extensive studies of properties and formation of nanotubes, but few of the use of an ultraviolet laser as the excitation source UV–Raman can not only diminish the fluorescence interference but also greatly enhance the Raman signal [Tair .P. C,et al.(1997).].m deal with the catalytic production of nanotubes. However, it seems this method is the best for producing carbon nanotubes at high yield. Raman spectroscopy is one of the most powerful techniques for characterizing catalysts because it can potentially obtain information about both surface adsorbed species and the structure of catalysts under working conditions. However, this technique suffers from two limitations: low Raman scattering signals and strong fluorescence that often obscures the weak Raman signal .However, carbon fiber exhibits a very poor oxidation resistance even at temperature as low as 700 K. Cylindrical carbon tubes were first discovered by transmission electron microscopy (TEM) over 50 years ago [Wang.Xu-zhen,et al.(2014).]. More recently, multi-walled carbon nanotube (MWCNT) composed of well-ordered graphene sheets were discovered in 1991 [Cao. X. H, Yin.et al.(2014).]. Since then, these carbon materials have been formally called ¨carbon nanotube¨ (CNT). Due to the unique chemical and physical properties of CNT, much research has been carried out on their growth mechanisms, structures, morphologies and their applications [Sinnott. S.B& Andrews. R.(2001).]. There have been several methods of CNT synthesis such as arc-vaporization [Liu .Y. Z, Chen. et al.(2014)]. laser ablation [Shi. J. L, et al.(2014).], and thermal chemical vapor deposition (CVD) [Hornyak. G.L,(1999)]. Since these edges constitute the main adsorbing surface, there is little under

that the bonded oxygen and hydrogen exercise a profound influence on the surface characteristics of carbons such as surface acidity [Xu.Y, et al.(2013). Wu.S & Chen.W,(2014) & Dong.X. et al.(2012). Cation exchange capacity [Flynn. J.H.(1996)&.Xu. Y. L, et al.(2001)] and adsorption of polar and nonpolar gases and vapors [Shinha.R.K& Walker.J.r. (1972).Lin.S, et al. (2001) & Yuan.J, et al.(2013)]. Carbon has various structures. Amongst the adsorbent materials, activated carbons are unique and versatile adsorbents because of their large surface area, micropore structure, varied adsorption effect, high adsorption capacity and high degree of surface reactivity. The carbon atoms located at the surface and edges of carbon crystallites have residual valences which make these atoms to act as active sites such as activated carbon, porous carbon [Bleda . M. J & Martinez J. M. (2008).],. Carbon black [Patil. U.M, Lee.S.C, Sohn.J.S, et al. (2014).], carbon nanotubes (CNTs) [Zhu.G, He. Z, Chen. J, et al. (2014).], diamond [Weng.K.W,et al.(2008).], carbon onions [Patil. U. M, Sohn. J. S, Kulkarni S B, et al.(2014)], etc. Carbon materials with controlled porosity can be prepared using various methods [Wang .G,et al. (2012)& Zhao.Y, et al. (2013)]. Three-dimensional materials with ordered porosity such as zeolites have been used to prepare carbon materials [Patil. U. M, et al.(2014) , Wang .G, et al(2012). & Zhao.Y, et al. (2013). Silicate clay minerals are layered materials that have also been used as templates to obtain porous carbons .They show a strong tendency to chemisorb other elements like oxygen, nitrogen, hydrogen, chlorine, bromine, iodine and sulfur and give rise to non-stoichiometric stable surface compounds called surface complexes. Among these surface complexes, surface oxygen complexes are the most common and most important. They are responsible for many physico–chemical and surface properties of carbons. X-ray examination of several carbons has shown that the oxygen atoms are bonded to the carbon atoms mainly at the edges of the giant molecules forming the aromatic sheets.

2.EXPERIMENTAL

2.1. Preparation Activated carbon.

Activated carbon, C in these papers from the solid waste "date pits" DP. AC was obtained from collected, washed by tap water, dried at 110 ^{0}C and crushed the date pits, DP. Carbon was prepared by subjecting the solid waste to direct steam pyrolysis at 800 ^{o}C two hour hold. The raw material was inserted into a stainless steel tube fitted with an internal wire diaphragm and held in a vertical position to dispose of the formed tarry matter. Heating of the pyrolysis tube was started to attain 350 ^{o}C for 35 min. then pure steam is admitted from top of the tube using a steam generator. After reaching 800 ^{o}C, the heated mass was left for 2 h at either temperature. The cooled activated carbon was weighed to determine burn-off and stored in tight glass containers. The weight loss was determined and referred to the original weight of precursor and denoted as "global burn-off" (GBO). Burn-off % = (weight of the raw material – weight of final product)/ weight of the raw material x 100.

2.2. Preparation of ZP materials by solid-solid reaction.

Zirconium phosphate has been prepared by solid-solid reaction[El-Said .N,et al,.(2001)]. The characterization of this inorganic ion exchanger was done with respect to capacity, pH titration, dissolution, etc. The pre-concentration and separation of fission products, Sr(II), Co(II), Eu(III), Gd(III), Hg(II) and Am(III) has been achieved from different acidic media, HCl, HNO_3, H_2SO_4, $HClO_4$. The speciation of these cations in different media has been investigated. From the results obtained, it is obvious that these cations can be pre-concentrated in low acidic medium, whilst at high acidity in the range 1-2 M, they be can separated from each other.

2.3.Reaction between $ZrCl_4$ and $NH_4H_2PO_4$

Definite weights of $ZrCl_4$, $2H_2O$ and $NH_4H_2PO_4$ were mixed and ground together with a molar ratio equal to n=(n=mole of $NH_4H_2PO_4$/mole of $ZrCl_4.2H_2O$)n=1,2,3.the girding and mixing were carried out for the reacting substances by agate mortar and pestle. The two compounds were ground and mixed thoroughly for 15min. chemical analysis was carried out of the produced mixture before and after washing with 4M HCl followed by distilled water and dried at 70^{o}C for 2 hours. Analysis of zirconium phosphate will be published.

2.4. Preparation of dopping material ZP in DP.

A mixture of ZP was mixed with DP with different ratios (0.1-0.9) and each sample was heated to 150 C ^{o} and the surface was measured by B.E.T. to choose the most suitable condition for studying parameters[El-Said .N,et al,.(2001)].

2.5. Techniques and Apparatus:

Infrared spectra were recorded from 4000cm−1 to 400cm−1 on a Brüker IFS 66v Fourier transform spectrometer using KBr pellets. The local chemical structure around phosphorus atoms was examined by solid-state 31P-

nuclear magnetic resonance under magic angle spinning conditions (MAS-NMR) spectroscopy on a Bruker MSL 300 spectrometer equipped with an Andrew type rotor rotating [El-Said.N, et al. (2014)]. The N_2 adsorption–desorption isotherms for dried powders were fixed Variation of pH of the solution as a function of time for NP in diluted nitric acid (6 g of NP in 100 ml of diluted HNO_3). **Figs. 1,2.** Percentages of dissolved P and Ca, as well as Ca/P ratio, after NP dissolution at various pH. Obtained by multi-point N_2 gas sorption experiments at 77K using a Micromeritics ASAP 2010 instrument. The specific surface areas were calculated according to the Brunauer–Emmett–Teller (BET) method using adsorption data in the relative pressure range from 0.05 to 0.25 whereas the pore size and volume were estimated using the Barret–Joyner–Halenda (BJH) approximation. Differential thermal analyses were carried out simultaneously in air flow using a TA Instruments Netzsch STA-409EP apparatus. The thermal measurements were conducted from 30 ◦C to 1200 ◦C with 10 ◦C/min as heating rate. The sample powder was chemically analyzed by inductively coupled plasma (ICP) emission spectroscopy (ICPS-7500, Shimadzu, Japan)**.** The FTIR spectra of the zirconium hydrogen phosphate, α-ZP, obtained at different speed agitation were shown in **Figure 2.** The spectra exhibit the characteristics vibration bands from the phosphate group. The broad band between 3435 and 3418 cm-1 has been attributed to asymmetric OH stretching of water molecule and the weak peak at around 1627 cm-1 indicates the bending of water molecule, which is not proportionate with the total intensity of the corresponding stretching band. A strong sharp band centered at 1062 cm-1 corresponds to P-O stretching vibration for ZP. The bands at 596 and 525 cm-1 attributed to deformations modes of PO_4^{3-} [Ge.J, et al.(2013)&Chen. M, et al. (2014)]. The distortionated band at 1060-1100 cm-1 in corresponds to some distorted tetrahedral phosphate groups in the nuclei of zirconium phosphates for the influence of the speed agitation during the forming of the products. In the case of ZP at 250 . It was observed one absorption band at 737 and 745 cm-1 respectively corresponding to P-O-P vibration of the diphosphate groups (O3P-OPO3). Finally, the observed bands to 1124 and 1113 cm-1 and 546 and 544 cm-1 from ZP500 and ZP250 correspond to the deformation vibrations of P-O bonding of the PO3 terminal groups.

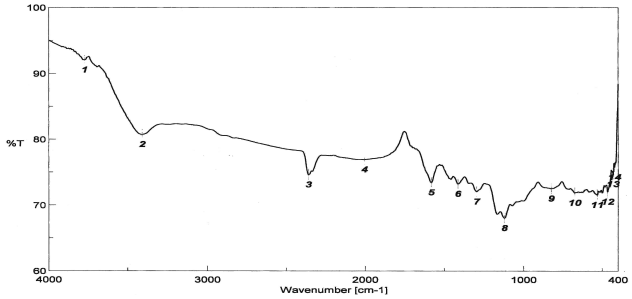

Fig.1. FTIR-Spectra of activated carbon obtained from DF by Chemical activation

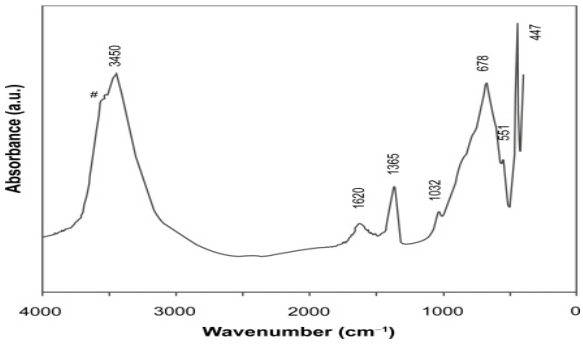

Fig.2. FTIR-Spectra for the ZP

2.6. SEM micrographs

It provides information on the structural changes in the date pits (DP) for analysis during the activation process. Figs (3a, 3b and Fig (4).Shows raw date pits (DP) before and after activation.and the shows the micrograph of AC at 500x magnification. The surface of DP is curly form resulted from the presence of cellulose, hemicelluloses and lignin in the raw material without any cracks. This would account for its poor or negligible BET surface area. The framework development was so rapid in resulting in extra cavities and leads to crack formation. Due to this well developed pores, the AC-50% possessed high BET surface area. Shows the micrograph of AC-50% at 5000x magnification. The micrograph magnifies the internal cavities, which are now clearly visible. Direct measurement from the micrograph shows that the average pore diameter is 5.23 µm. The surface of the AC- 50% seems to be clearer and smoother than DP surface due to the removal of volatile compounds and impurities during the activation process and followed by H_3PO_4 wash. It can be seen that there are solid appeared in the pores of AC- 50% where some small white particles are scattered on the surface of the carbon, may be due to the remains of the H_3PO_4 which was not washed completely during the activation**.**

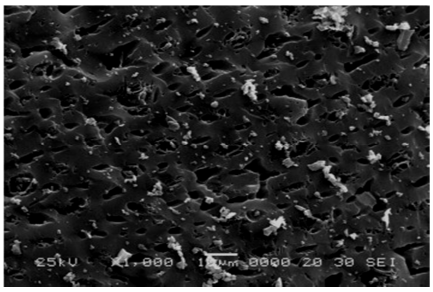

3a-AC

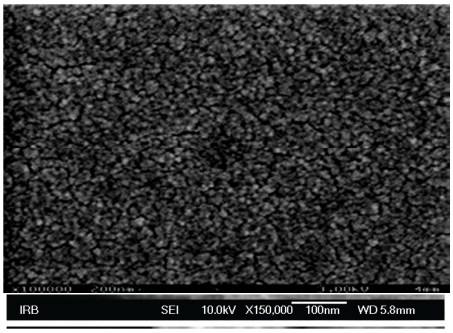

3b-Zp

Zp+AC

Fig.4.SEM for AC, B(ZP) and C (AC +ZP.)

3. RESULTS AND DISCUSSION

The carbon–nanoparticles/nanocomposites have been the exponentially growing field of research for developing the materials in last few decades and have been mainly focusing on the structure–property relationships and their development. Since the carbon–nanocomposites have been the staple of modern carbon industry, their durability under various environmental conditions and degradability after their service life are also essential fields of research. In very few systems, the nanoparticulates have been incorporated into carbons '**nano-additives'** for both purposes: degradation and stabilization of carbons. This simple, eco-friendly and cheap procedure may be useful for the future development of nanomaterials for The field of nanoscience and nanotechnology is extending the applications of physics, chemistry, biology, engineering and technology into previously unapproached infinitesimal length scales. This simple, eco-friendly and cheap procedure may be useful for the future development of materials in bone fabrication. This work demonstrates that it is possible to obtain nanoporous apatite phases using natural phosphate as calcium and phosphate sources. Noticeably, the highest surface area is obtained when the synthesis is performed at room temperature and without organic additive. This method shows a number of advantages: (a) compared to double precipitation or neutralization methods, it does not involve an extensive use of chemicals but can be performed from an abundant raw material,

representing an important gain in terms of cost; (b) the dissolution–precipitation method can be performed without heating and without organic solvent, so that not only this process is eco-friendly but also the final materials are free of organic impurities, an important issue for their application for water treatment in natural environment.

3.1. Characterization of activated carbon.

This was achieved by the standard adsorption of N_2 at 77k, using a sorpatometer of the type NOVA 1000e (Quanta chrome). In spite of limitations of the BET method, in case of activated carbon, it has been and will continue to be used for microporous adsorbents owing to its simplicity and reasonable [El-Said .N,et al (2001).]. Accordingly, the adsorption isotherms were analyzed to get various porous parameters: By applying the BET-equation to determine the S_{BET} surface area, total pore volume (V_P), from amount of nitrogen held at P/P^0 =0.95, and average pore dimension (radius) from $R=2V_P/ S_{BET}$ was evaluated. Other porous characteristics were estimated from the t-plots constructed by plotting volume of gas adsorbed (V_a) versus t-values of adsorption on non-porous standard carbon as reported by Selles-Perez and Martin-Martinez [Chen. M, et al. (2014)]. The obtained α s-value was transformed into t-values by multiplication with 1.52 x 3.54 (Å) as suggested by the same authors. The following porosity characteristics were calculated as follows: total surface area (S_t) from slope of early straight line to zero, non-microporous surface area (S_n) from slope of the late straight portion, ultra micropore volume (V_{0u}) from early intercept of the base straight portion, and super micropore volume (V_{os}) from the late intercept of the base straight portion with V-axis.

3.2. Fourier Transform Infrared Spectroscopy (FTIR) analysis

The FTIR spectra can provide valuable information about the chemical compositions of the materials**. Figure 1** shows the comparison FTIR spectra of raw date frond (Raw-DF), AC of date frond at 60% concentration of H_3PO_4 (AC-60%) and commercial activated carbon (AC-C) for comparison. Raw date frond (DF) in **Figure 1** shows the most complicated and apparent spectrum. A strong and broad adsorption peak appeared at 3434.06 cm-1, which corresponds to the stretching of O – H functional group and this shows the presence of bonded hydroxide in the raw sample. There was another peak observed at 2930.44 cm-1 corresponding to the C – H sp3 stretching. A strong conjugated C=C peak also observed around 1633.83 –1638.32 cm-1. This sample also shows four important absorption peaks at 1251.06, 1160.53, 1113.89 and 1053.53 cm-1 respectively which represent the stretching of C – O functional group. It can be suggested from 27 the spectrum that the main oxygen groups present in the raw-DF are carbonyl, ethers and alcohols group which are normally present in plant cellulose. In contrast to the FTIR spectrum shown by raw -DF, the spectrum AC-60% and AC-C illustrate less absorption peaks clearly, most of the absorption peaks of functional groups were diminished. Basically all the samples show a weak broad peak around 3425.12 –3440.32 cm-1, which indicates the presence of OH in the samples. It is most probably of the R-OH bonded like molecule in carbon. Finally, the spectra for the prepared activated carbon from date's frond chemical activated at 60% H_3PO_4 when comparable to the commercial AC, there seem a great similarity. This might indicate that the prepared AC is of similar in grade and standard of that the commercial prepared carbon nano tubes[Ge.J,et al(2013)].

3.3. Nonthermo for nano technology.

The prepared sample of nano materials shows the maxmiun of Zp/DP at 0.1 and the studying TGA at this ratio shows the suitable temperature of nano material befor starting decomposition at 150 C ^{o}. From optimization the order and activation of reaction ws studied conditions where Zp/DP and T 150 ^{o}C $\cdot$ Therefore the kinetics of complex reactions, where the reaction model changes with the extent of reaction, can be analyzed with CR method. In most of solid state reactions (especially solid-solid reactions), a layer of products forms on the surface of un-reacted core and in porous. This layer may be porous or dense and this causes a change in the reaction mechanism by the increase in extent of reaction. Thus the CR method is effectual method in kinetic analysis of solid state reactions.

3.4. Single point BET Surface Area of Activated Carbon

The single point BET surface area analysis was done to study the effect of different activation method on the surface area of carbon samples. All the data collected, including the raw-DF, AC-60% and AC presented in the form a chart in **Figure.4.** A1, A2.Raw DF gives only 4.6 m^2g^{-1} of BET surface area and for AC-60% is 1139 m^2g^{-1}. Comparatively, the synthesized samples exhibit slightly higher surface area than the commercial activated carbon which only 1069 $m2g^{-1}$. This result proposed that the chemical activating agent used, H_3PO_4 has contributed to the higher surface area as compared to the commercial activated carbon.

3.5. Statistical analysis

Three separate studies were performed. Assays were run in triplicate for each material and at each time point and the data were analyzed using Student's t-test as described previously [Chen. M, et al. (2014).Tarafdar.A`; et al,& Wu. Q, et al. (2011)] and significance considered achieved at po0:05:The surface area was determined according to langmuir, alpha and beta method was shown in **tables(1,2).**

Table.1.Surface characteristics of activated carbons (ACs) ,(ZP) and (ACs+ZP)50% obtained by chemical and physical activation.

Material	S_{BET} m^2/g	S^{α}_{t} m^2/g	S^{α}_{n} m^2/g	V_P ml/g	V_{meso} ml/g	V_{ou} mL/g	V_{ot} ml/g	V_{os} ml/g
ACs(100%)	1066.02	1134.9	542.9	0.875	0.588	0.002	0.287	0.287
ZP(100%)	400	110	410	0.375	0.422	0.001	0.110	0.123
ACs +50% ZP	800	112	450	0.556	0.4512	0.002	0.1586	0.1522

Table 2. Surface characteristics of ACs, mixed with different ratios of the ZP

Type of ZP	Langmuir surface area S_L (m^2/g)	Average pore radius ŕ (Å)
ZP only	91.67	3.412
10%C	179.06	3.102
20%C	314.18	3.042
30%C	451.58	3.008
40%C	609.38	2.992
50%C	709.19	2.912
Carbon only	1688.42	3.27
10% ZP	1260.09	2.89
20% ZP	1129.40	2.966
30% ZP	950.53	2.902
40% ZP	889.78	2.88
50% ZP	709.19	2.912

3.6. Structure and thermal stability correlation

The TGA and DTG data reveal that although the molecular composition of the ZP-C is different, the nature of the decomposition pattern is different. The ZP material exhibits three-stage decomposition whereas two-stage decomposition is observed in the case of nitrate complexes. Within the series the phosphate material is the least stable and the phosphate material is the most stable. The difference in thermal **Table(2).**Surface characteristics of ACs, mixed with different ratios of the ZP **.**

3.7. Mechanistic aspects

The assignment of the mechanism is based on the assumption that the form of g(α) depends on the reaction mechanism. Here in the present investigation, nine forms of g(α), suggested by Satava [Satava Vecchio et al.(2003)] are used to enunciate the mechanism of thermal decomposition in each stage.The correlation coefficient for all these nine forms were calculated and the form of g(α) for which the correlation has a

maximum value is chosen as the mechanism of reaction. In the present investigation, the highest value of correlation coefficient is obtained for the equation{1}, in all stages of decomposition. Hence, the mechanism is "random nucleation with one nucleus on each particle" representing 'Mampel model' as in equation (1).

$$g(\alpha) = -\ln(1-\alpha) \quad \text{.....(1)}$$

3.8. Kinetic aspects

All the well-defined stages were selected for the study of the kinetics of decomposition of the complexes. The kinetic parameters (the activation energy E and the pre-exponential factor A) were calculated using the Coats-Redfern equation (2), [He.Y.M, et al.(2013)].

$$\log\left[\frac{g(a)}{T^2}\right] = \log\frac{AR_s}{\phi E}\left[1-\frac{2RT}{E}\right] - \frac{E}{2.303RT} \quad \text{..... (2)}$$

In the present case, a plot of L.H.S of this equation against 1/T gives straight line (Figs.5 and 6) whose slope and intercept are used for calculate the kinetic parameters by the least-square method. The goodness of fit was checked by calculating the correlation coefficient. The entropy of activation S can be calculated using the equation (3).

$$A = \frac{kT_s}{h} e^{\Delta S/R} \quad \text{..... (3)}$$

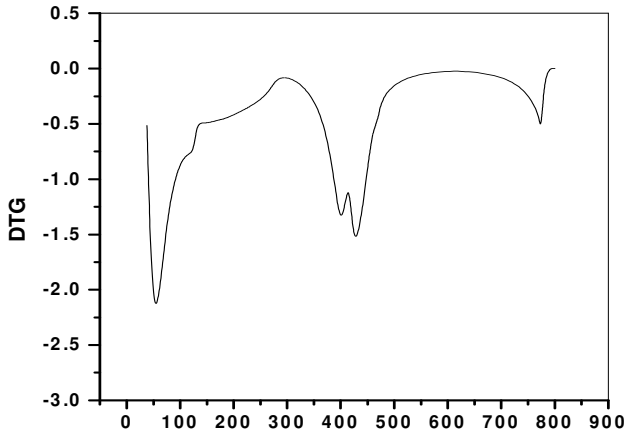

Fig(5): Thermogravemetric analysis (DTG) against temperature .

A1

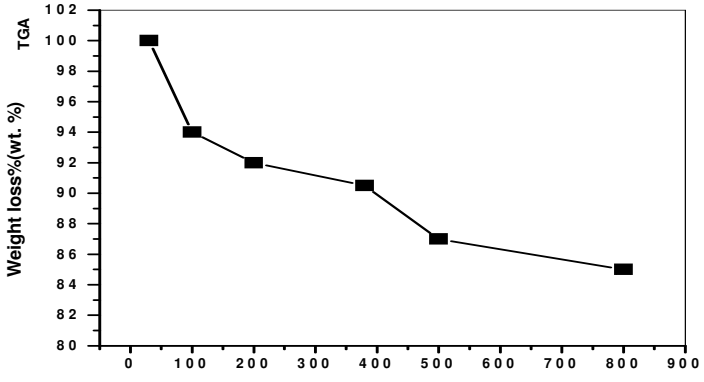

Fig(6):Thermogravemetric analysis (TGA) against temperature

A2

Where, k is the Boltzmann constant, h is the Planck's constant and T_s the peak temperature. The various kinetic parameters calculated are given in Table 2. The activation energy (E) in the different stages are in the range 30.16–306.99 kJ mol−1. The respective values of the pre-exponential factor (A) vary from 2.72×10^{-2} to $7.84\times107\ s^{-1}$. The corresponding values of the entropy of activation (S) are in the entropy.

$$\frac{-\frac{E}{2.3R}\Delta\left(T^{-1}\right)}{\Delta\log\left(W_r\right)} = n + \frac{\Delta\log\left(\frac{dW}{dt}\right)}{\Delta\log\left(W_r\right)} \quad \text{..... (4)}$$

$$\log\left[\frac{1-(1-\alpha)^{1-n}}{T^2(1-n)}\right] = \log\frac{AR}{aE}\left[1-\frac{2RT}{E}\right] - \frac{E}{2RT}$$

Freeman–Carroll [Huang. H, et al. (2014)]. Showed that the kinetic parameters of any decomposition process could be calculated from the thermo analytical curve using the relation where E is the energy of activation, T is the absolute temperature, R is the gas constant, W_r is the mass loss at completion of reaction minus mass loss upon time, n is the order of reaction and dW/dt is the rate of mass loss with time. The plot of $[\log(dW/dt)]/\log W_r$ vs. $(T^{-1})/\log W_r$ gives a straight line with intercept –n and slope (E/2.3R).The values of the activation energy and the order of reaction are given in Table(1).The activation energies and order of reactions were also calculated by Coats–Redfern [Wu.S, et al. (2014)].According to all values of n except = 1, where n is the order of reaction, is the fraction decomposed, T is the temperature in K, A is a frequency factor, R, K are the gas constant, is the heating rate in degree per minute and E is the energy of activation. The plot of $\log\{[1-(1-n]/[T^2(1-n)]\}$ vs $1/T$ gives a straight line of slope –E /2.3R for the correct values of n for most values of E and for the temperature range of any reaction, the expression [AR/(aE)](1-2RT/E) is sensibly constant. The variations in the calculated activation energies are given in Tables 3 . Coats and Redfern (CR) calculations can be used to investigate one series of samples and detect any variation in the activation energy. The values of n from either Freeman–Carroll calculations or Coats–Redfern calculate ns given in Tables 3 seemed to be reasonable. The calculated order of reaction of doping ZP in activated carbon was 2 due to its organic constituents and ZP that thermally decompose.[Huang., et al. (2014).Chen. M, et al. (2014). Yu .P. P, et al. (2014).& Ju. H. F, et al (2014)].

Table.3.Rate parameters calculated from thermodynamic data for ZP(Zirconium phosphate) using thermo gravimetric analysis (TGA)

	Freeman–Carroll		Coats–Redfern	
ZP%	n	E/kJ mol^{-1}	n	E/kJ mol^{-1}
5	2	292	2.03	289
7	2	291	2.08	285
20	2.	294	2.15	297
40	2	290	2.98	292

Based on the data, it may be concluded that the preparation of nanomaterial Zr- carbon take place in either carbon ZP in a temperature range 22–150°C. Doping of ZP in Carbon increases the stability of ZP. As the concentration of doped ZP increases the total mass loss of the matrix decreases. Doping of ZP in carbon increases the thermal stability of the solidified matrix. According to the kinetics of Freeman–Carroll and Coats–Redfern the calculated order of reaction of ZP is 2. The calculated activation energy of both matrices are 231 kJ mol-1The % of decomposition for DP, 0.1, Zp, 0.5ZP,Zp are at different temperatures ae shown in Fig.5. and the decomposition follow the order Zp> DP > 0.1,Zp >,0.5ZP in the range (150-900)^{0}C,while it the same in the range 0=150 ^{0}C,Fig.5..A1.Thermogravemetric analysis (DTG) against temperature for 0.1ZP+0.9 AC A2. DTA againt temperature for 0.1ZP+0.9 ACThe relations between the ZP/DP ratio and average pore diameter is shown in Fig .6. It depicts that the maximum average diameter (A^o) at ZP/DP ratio equal $0.5A^0$ .The minimum average diameter (A^o) at ZP/DP ratio equal 1 while The relation ZP/Dp and the surface area is shown in T temperature 150 C^0 was shown in Fig.7. giving apolynomial series $\%S = A + B1*ZP/DP+B2*X^2$ where S is the surface area X=ZP/DP ,B1 and B2 are consists solving ,of this equation A=29.,B= B1=-1,11 B2=0.011 , plot of ZP/DP as X-axes ,Y is the average pore diameter, For optimization ,The 3D.Shown that 3-D Fig(8a,3-D)plot of ZP/DP as X-axes ,Y is the average pore diameter,Z is the surface area and Fig.8a while the contour plot in Fig.8B**.** ZP/DP as X-axes, Y is the average pore diameter .the maximum average diameter (A^o) at P/DP Zp/D

ratio equal 0.1 D optimization Fig.8a while The contour plots Fig.9.B.to show the critical area for preparation of nonomaterial of dopping ZP in DP.

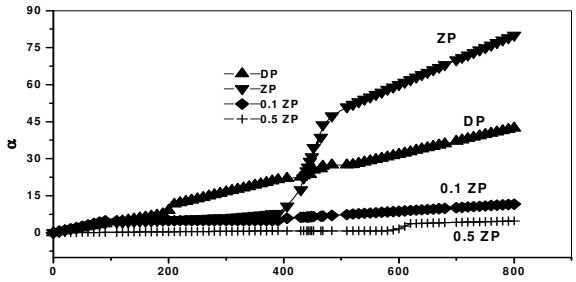

Fig.7: Fraction decomposition of DP
,ZP,10%ZP+90%DP and 50%ZTP+DP and DP

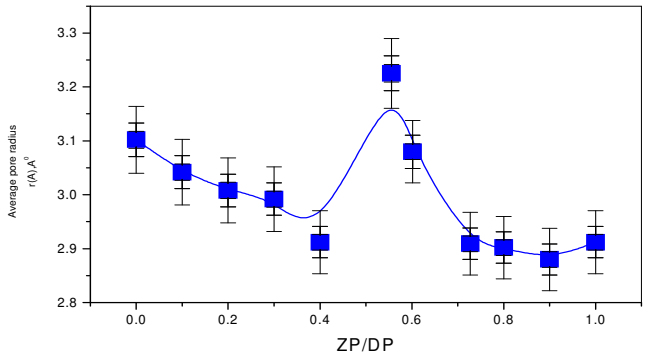

Fig .8.The relation between the Zp/DP ratio and average pore diameter

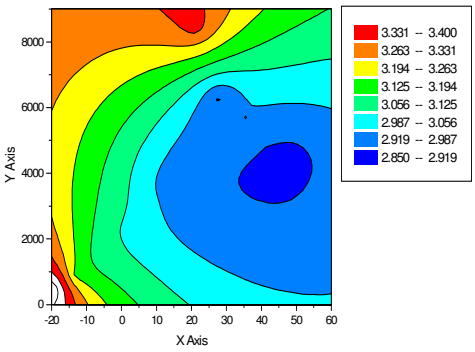

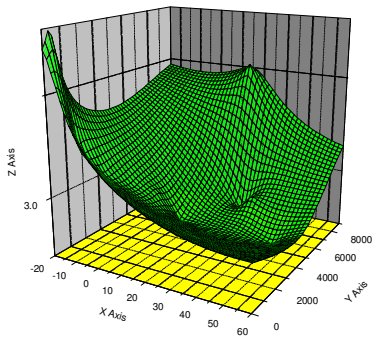

Fig.8.aThe 3-D optimization Fig.8.B.The contour plots.

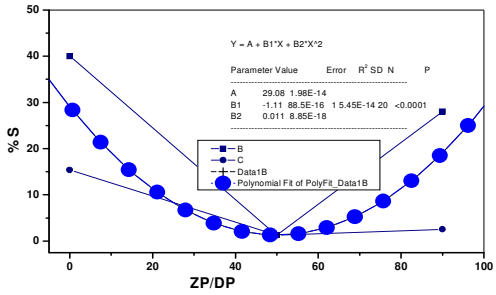

Fig.9..Critical area of preparatiion nanoparticles of ZP and ACs in mesopores of DP

CONCLUSION.

A nano hybrid thermal material can be prepared at 150 C^0 via doping of zirconium phosphate which is prepared by solid-solid reaction –in activated carbon to obtain very high surface area 1260.09 S_L (m^2/g) and Average pore radius ŕ (Å)3.27 and minimum particle size . The Kinetic aspects was studied by the kinetics of Freeman–Carroll and Coats–Redfern the calculated order of reaction of ZP is from TGA.The Structure and thermal stability correlation .A Statistical analysis and Mechanistic aspects was confirmed by FTIR and SEM analysis. The thermo nano material can be used in separation of radioactive isotopes and organic pollutants from fission products with high efficiency and fast reactions .The work is conducting for studying a separation processes from radioactive waste and envioronment .

REFERENCES

[1] Flynn,J. (1992) "Thermal analysis kinetics"32,Elesiver,232:519-26.
[2] House,J. (1990) "Kinetics and mechanism of the dehydration of ammonium"36,Elesiver, 89-155.
[3] Ozawa, T. (1965) "Nonisothermal kinetics by thermal analysis "266.CSJ,1881-6.
[4] Flynn, J,H.(1996) " Measurement of the Thermodynamic Properties of Multiple"33,Elesiver, 282-283.
[5] Xu Y, L., Cheng, L., et al (2001)" Surfactant-Free Emulsion-Based Preparation of Redox-Responsive Nanogels"58, Elesiver,196–202.
[6] Yin,Y., Binner,J., G & Cross, T., E.(1994) " Protective SiC Coating on Carbon Fibers by Low Pressure"29,Elesiver, 2250–2254.
[7] Zhao. L.R, Jang. B. Z. (1997). The oxidation behavior of low-temperature heat-treated.J. Mater Sci.32(11), 2811–2819.
[8] Bullions,T.,A, McGrath J,E & Loos, A., C (2003) " numerical model to predict fiber tow saturation during liquid composite".439,Elesiver,1737–1748.
[9] Labruquére,S., Gueguen, J., S& Pailler,R.(2002)" Carbon fiber ceramic matrix composite, Anti-oxidation". 22,Elesiver,1023–1030.
[10] Tair, P., C& Li,C. (1997)" Ultraviolet Raman spectroscopy of catalysts and other solids".77, Scitation , 1679–84.
[11]Wang,.Xu.,zhen, Liu .,&Ning, Hu.(2014) "Fabrication of three dimensional MoS2-graphene hybrid monoliths and their catalytic performance for hydro desulfurization". 119,Elesiver, 81-88.
[12] Cao, X., Yin H, Z., Y& Zhang,H.(2014) "Three-dimensional graphene materials: preparation, structures and application in super capacitors".8,Elesiver, 1850-1865.
[13] Sinnott,S.,B&Andrews,R(2001) "Carbon nanotubes: synthesis, properties, and applications" .10,Elesiver,145–249.
[14] Liu, Y., Z, Chen C, M & Li ,Y., F (2014) "Crumpled reduced graphene oxide by flame-induced reduction of graphite oxide for supercapacitive energy storage"6,Elesiver, 5730-5737.
[15] Shi J, L., Du W, C & Y, X., Yin (2014)" Hydrothermal reduction of three-dimensional graphene oxide for binder-free flexible supercapacitors"6,Elesiver, 10830-10834.
[16] Hornyak,A., Dillon ,A., C ., Parilla P, A., Schneider, J, J., Czap,N & Jones, K., M (1999)". Template synthesis of carbon nanotubes"57, Hindawi Publishing.,83–88.
[17] Xu,.Z.,Y & Huang, X (2013)." Flexible solid-state supercapacitors based on three-dimensional graphene hydrogel films".89,ACS., 4042-4049.
[18] Wu,S., Chen, W & Yan, L (2014)".Fabrication of a 3D MnO2/graphene hydrogel for high-performance asymmetric supercapacitors"56,Elesiver, 2765.

[19] Dong,X.,C, Xu, H & Wang, X.,W (2012) "3D graphene-cobalt oxide electrode for high-performance supercapacitor and enzymeless glucose detection"79, ACSN,3206-3213**.**
[20] Shinha, R,K & Walker, J., r (1972) "Chemisorption of oxygen on carbon sites followed by reaction with i-isS. Throughout"11,Elesiver, 754-61.
[21] Lin, S, C., C, Khoh & Reynolds, A, S (2001)" Recovery of used frying oils with adsorbent combinations; Refrying and frequent oil replenishment"243,Springer,159-169.
[22] Yuan,J., Zhu.,J & Bi,H (2013) "Graphene-based 3D composite hydrogel by anchoring Co3O4nanoparticles with enhanced electrochemical properties".Elesiver, 12940-12945.
[23] M J Bleda & J M Martinez (2008) Effect of surface chemistry on electrochemical storage 3 of hydrogen in porous carbon materials.J. Carbon,31: 1053.
[24] Patil, U., M , Lee, S.,C & Sohn, J., S (2014) "Enhanced symmetric supercapacitive performance of Co(OH)2nanorods decorated conducting porous graphene foam electrodes". 129,Elesiver, 129334-342.
[25] Zhu,G, He, Z & Chen .,J (2014) "Highly conductive three-dimensional MnO2-carbon nanotube-graphene-Ni hybrid foam as a binder-free supercapacitor electrode"Wiely, 1079-1085.
[26] Weng, K., W, Han,S., Chen, Y., C & Wang, D., Y (2008) "Nanodimensional and nanocrystalline Apatites and Other Calcium Orthophosphates in Biomedical Engineering, Biology and Medicine". 226,Elesiver, 117-125.
[27] Patil, U., M, Sohn. J, S & Kulkarn, S., B (2014) "Enhanced supercapacitive performance of chemically grown cobalt-nickel hydroxides on three-dimensional graphene foam electrodes"ASC,2450-2458.
[28] Wang, G & Zhang.,L(2012) "A review of electrode materials for electrochemical supercapacitors"116,ASC, 797-828.
[29] Zhao,Y., Liu,J & Hu ,Y(2013)"Highly compression-tolerant supercapacitor based on polypyrrole-mediated graphene foam electrodes"Elesiver, 591-595.
[30] El-Said,N & Siliman,A,M., (2001) **"**Separation and speciation of fission products by zirconium phosphate prepared by solid-solid reaction".89,Elesiver,89: 647**.**
[31] El-Said, N & Ali, M., M (2014) "Nanoapatite for Nanotechnology: part (III) A novel process for the fabrication and Improvement of nanoporous". Hindawi, 93-102.
[32] Ge,J.,,H, Yao, B & Hu ,W (2013) "Facile dip coating processed graphene/MnO2nanostructured sponges as high performance supercapacitor electrodes"33,Elesiver, 505-513.
[33] Chen, M & Wang ,H " (2014) Novel and facile method, dynamic self-assemble, to prepare SnO2/rGO droplet aerogel with complex morphologies and their application in supercapacitors".118, ACS, 14327-14337.
[34] Tarafdar,A., Panda, A., B, Pradhan ,N., C & Pramanik, P (2006) "Synthesis of spherical mesostructured zirconium phosphate with acidic properties"220,Elesiver, 360-365.
[35] Wu,Q., Sun.,Y & Bai,H (2011)" High-performance supercapacitor electrodes based on graphene hydrogels modified with 2-aminoanthraquinone moieties"48,Elesiver, 11193-11198.
[36] Satava Vecchio (2003) "Thermogravimetric and kinetic methods to date wood finds". 39,Elesiver,897–907.
[37] He, Y.,M, Chen ,W., J & Li, X., D (2013)."Freestanding three-dimensional graphene/MnO2composite networks as ultra light and flexible supercapacitor electrodes"7,ACS, 174-182.
[38] Huang,H., Xu,L & Tang, Y (2014)" Facile synthesis of nickel network supported three-dimensional graphene gel as a lightweight and binder-free electrode for high rate performance supercapacitor application"6,Springer, 2426-2433.
[39] Chen,M., & Li,L (2014)"Novel and facile method, dynamic self-assemble, to prepare SnO2/rGO droplet aerogel with complex morphologies and their application in supercapacitors".6,ACS,14327-14337.
[40] Yu, P., P, Zhao,X & Huang,Z.,L (2014) "Free-standing three-dimensional graphene and polyaniline nanowire arrays hybrid foams for high-performance flexible and lightweight supercapacitors"7,Elesiver,: 14413-14420.
[41] Ju, H., F , Song W, L & Fan, L., Z (2014) "Rational design of graphene/porous carbon aerogels for high-performance flexible all-solid-state supercapacitors"56,Elesiver, 10895-10903.